



Particulate organic matter as causative factor to eutrophication of subtropical deep freshwater: Role of typhoon (tropical cyclone) in the nutrient cycling

Xiaofei Gao^{a,b}, Huihuang Chen^{a,b}, Binhe Gu^c, Erik Jeppesen^{d,e,f,g}, Yuanyuan Xue^a, Jun Yang^{a,*}

^a Aquatic EcoHealth Group, Fujian Key Laboratory of Watershed Ecology, Key Laboratory of Urban Environment and Health, Institute of Urban Environment, Chinese Academy of Sciences, Xiamen 361021, China

^b University of Chinese Academy of Sciences, Beijing 100049, China

^c Soil and Water Science Department, University of Florida, 106 Newell Hall, Gainesville, FL 32611, United States

^d Department of Bioscience, Aarhus University, Vejlsovej 25, 8600 Silkeborg, Denmark

^e Sino-Danish Centre for Education and Research, Beijing 100049, China

^f Limnology Laboratory, Department of Biological Sciences and Centre for Ecosystem Research and Implementation, Middle East Technical University, Ankara, Turkey

^g Institute of Marine Sciences, Middle East Technical University, Mersin, Turkey

ARTICLE INFO

Article history:

Received 11 July 2020

Revised 25 September 2020

Accepted 26 September 2020

Available online 28 September 2020

Keywords:

Organic matter

Deep water mixing

Microbial loop

Multi-nutrient cycling index

Stable isotope

Stoichiometry

ABSTRACT

Intense storms pose a serious threat to ecosystem functioning and services. However, the effects of typhoons (tropical cyclones) on the biogeochemical processes mediating risk of eutrophication in deep freshwater ecosystems remain unclear. Here, we conducted a three-year study to elucidate linkages between environmental change, stable isotopes and the stoichiometry of particulate organic matter (POM), and nutrient cycling (i.e., carbon, nitrogen and phosphorus) in a subtropical deep reservoir subjected to typhoon events. The typhoons significantly changed the nutrient levels in the deep waters as well as the thermocline position. Increased typhoon-driven organic matter input, algae sinking and heterotrophic decomposition interacted with each other to cause steep and prolonged increases of total nitrogen, ammonium nitrogen and total phosphorus in the bottom waters of the reservoir. Small-sized or pico-sized POM (i.e., 0.2–3 μm) showed a substantial increase in bottom waters, and it exhibited stronger response than large-sized POM (i.e., 3–20, 20–64, 64–200 μm) to the typhoons. Our results also indicated that typhoons boost the nutrient cycling in deep waters mainly through pico-sized POM.

© 2020 Elsevier Ltd. All rights reserved.

1. Introduction

In tropical and subtropical regions, the intensity of typhoon events (also termed tropical cyclones or hurricanes) are expected to increase as a consequence of the ongoing climate changes as well as to cause economic and ecosystem functioning losses due to the strong wind and torrential rain (Mumby et al., 2011; Coumou and Rahmstorf, 2012; Fang, 2016; Emanuel, 2020). Deep reservoirs and lakes are typically characterized by algae-rich surface waters (epilimnion) and potential nutrient-rich bottom waters (hypolimnion) (Boehrer and Schultze, 2008; Yu et al., 2014). Wind-induced mixing disturbances can bring the hypolimnetic nutrients up into the photic zone, and heavy precipitation may lead

to an increase in the influx of terrestrial material, including nutrients, into these waterbodies (Paerl et al., 2006; Sinha et al., 2017). Such pulse disturbances are typically accompanied by an increased algae biomass or a shift in the plankton community composition (Tseng et al., 2013; Ji et al., 2018; Stockwell et al., 2020). However, the underlying processes and mechanisms driving the variations of plankton community after typhoon are difficult to estimate from typical low-frequency monitoring. High-frequency observations using novel methodology, however, may enhance our understanding of the biogeochemical processes following episodic climatic disturbances in freshwater ecosystems in an increasingly changing world.

The stoichiometry and stable isotopes of particulate organic matter (POM) are useful tools for the understanding of the biogeochemical processes associated with plankton dynamics and eutrophication processes (Leal et al., 2017; Glibert et al., 2019). The

* Corresponding author.

E-mail address: jyang@iue.ac.cn (J. Yang).

stoichiometric variations of grazer and algae can influence the rates of nutrient release, altering the structure and functioning of freshwater ecosystems (Elser and Urabe, 1999). Stable isotopes of POM have been widely used to study the biogeochemical processes and to track element sources (Fry, 2006; Gu, 2009; Gu et al., 2011; Glibert et al., 2019). The stable carbon isotope ($\delta^{13}\text{C}$) of POM is considered as a good proxy for CO_2 concentration and primary production, and stable nitrogen isotope ($\delta^{15}\text{N}$) can be used as indicators of the N_2 fixation process and trophic position along a food chain in lakes (Gu et al., 2006; Trochine et al., 2017). Therefore, the temporally and spatially integrated information on biogeochemical processes provided by stable isotopes and the stoichiometry of POM are important for understanding the nutrient cycling in freshwater ecosystems following typhoon events.

The size of POM is an important functional trait, as it affects the bioavailability and biogeochemical cycles of nutrients in aquatic ecosystems (Woodward et al., 2005). POM mainly consists of plankton and dead organic matter (Moore et al., 2004). The sizes of most free-living bacteria are typically $< 3 \mu\text{m}$, while most planktonic algae are larger and within the range $3\text{--}20 \mu\text{m}$, and most protozoans and metazoan are $> 20 \mu\text{m}$ and $> 64 \mu\text{m}$, respectively (Ch  telat et al., 2006). The responses of plankton to typhoon-driven disturbances vary among size classes and along the water column (Jones et al., 2008; Ji et al., 2018). In a natural lake, Jones et al. (2008), for example, found that the bacterial community composition recovered fast after a typhoon disturbance, while the algal communities did not. Moreover, microbial communities exhibited a higher ability to recover from an artificial mixing disturbance in the surface waters than in the deep waters (Shade et al., 2012). Therefore, studies should not only focus on the microbial communities in the surface waters but also explore the potentially prolonged responses of the microbially mediated biogeochemical processes in the deep waters following strong winds (e.g., typhoons).

Stoichiometry plays a key role for the nutrient cycling and community composition (Sardans et al., 2012). The C:P ratio of organic matter, for example, can greatly influence the global nitrogen fixation rate (Wang et al., 2019). The multi-nutrient cycling index (i.e., carbon, nitrogen and phosphorus) has been used to address the importance of different taxonomic groups for the nutrient cycling in terrestrial ecosystems (Delgado-Baquerizo et al., 2016; Jiao et al., 2018). However, less is known about the contribution of key drivers and the implications of different POM size classes for the multi-nutrient cycling in freshwater ecosystems, especially following typhoon events.

We explored the susceptibility and drivers of nutrient cycling using meteorological and physicochemical variables, stable isotopes and the stoichiometry of different POM size classes following typhoon events in a subtropical reservoir (Fig. S1). We focused on the two questions: (1) How did the typhoon affect the biotic and abiotic conditions in different water layers of the reservoir? (2) Which size fraction of POMs can be a key indicator of changes in nutrient cycling? To answer these questions, we explored the environmental change throughout the water column during one month before and after typhoon events in Tingxi Reservoir in southeast China. We then assessed the importance of different POM size classes for the multi-nutrient cycling using the stable isotopes and stoichiometry of POM. We hypothesized that (1) POM changes (concentration and size) driven by the typhoon events would differ among the different water layers, and that (2) POM would be a key contributor to the nutrient cycling, differing though in importance among particle size classes and water layers. This study highlights the importance of using stable isotopes and stoichiometry of POM to elucidate the nutrient cycling in different water layers and provides new insight into the biogeochemical processes of freshwater ecosystems following typhoon events.

2. Materials and methods

2.1. Study site and sampling processes

A three-year (2015–2017) field sampling campaign was conducted near the dam of the Tingxi Reservoir ($24^\circ48'\text{N}$, $118^\circ08'\text{E}$) in Xiamen city, Fujian province, southeast China. Tingxi Reservoir was built in 1956 and has a drainage area of about 100 km^2 and a total storage of $48 \times 10^6 \text{ m}^3$ (Yang et al., 2012). The trophic state of the reservoir was light eutrophic level with a trophic state index ranging from 50.8 to 56.3, which were calculated using chlorophyll-*a*, Secchi depth and total phosphorus (Yang et al., 2012). The reservoir is deep with surface chlorophyll-*a* concentrations ranging from 9.5 to $22.2 \mu\text{g dm}^{-3}$. Details of the reservoir are given in our previous studies (Yang et al., 2012, 2016; Gao et al., 2019). Annual mean precipitation is about 1336 mm and annual mean temperature 20.7°C (Liu et al., 2019). Xiamen is characterized by a subtropical monsoon climate and is located at the westbound belt of typhoon movement in the northwestern Pacific Ocean. Typhoons are a common disturbance of the Tingxi Reservoir, especially during the water stratification period in summer and autumn.

Samples of particulate organic matter (POM) were collected every 20 days (every 10 days in September 2016 after the typhoon Meranti) from 2015 to 2017. Samples were collected from the sub-surface layer (depth, 0.5 m), the hypoxic boundary (depth, $21\text{--}27 \text{ m}$) and subbottom layer (2 m above the bottom sediments) (Fig. S1a, b). POM was partitioned into four size classes (fractions): $0.2\text{--}3 \mu\text{m}$ (pico-sized), $3\text{--}20 \mu\text{m}$ (nano-sized), $20\text{--}64 \mu\text{m}$ (micro-sized) and $64\text{--}200 \mu\text{m}$ (net-sized). Briefly, we pre-filtered the samples through $200 \mu\text{m}$, $64 \mu\text{m}$ and $20 \mu\text{m}$ nylon sieves *in situ*, followed by sequential filtering through $3 \mu\text{m}$ and $0.2 \mu\text{m}$ pore-size polycarbonate filters (47 mm diameter, Millipore, Billerica, MA, USA) in the laboratory. The samples were then gently backwashed from filters into 15 cm^3 plastic centrifuge tubes. Finally, all the samples were freeze-dried at -80°C for at least 72 h prior to nitrogen and carbon elemental and isotopic analyses.

2.2. Meteorological data collection

Fujian province is a perfect region for studying typhoon-induced disturbances (Sajjad et al., 2019). We focused on typhoons within a $< 300 \text{ km}$ distance from the typhoon center to the Tingxi Reservoir (Table S1; Fig. 1). Data on air temperature (AT), precipitation and wind speed (WS) were collected from China Meteorological Data Service Center (<http://data.cma.cn>) (at station Xiamen ID 59,134; coordinates $24^\circ29'\text{N}$, $118^\circ04'\text{E}$). To evaluate the effect of typhoon, we applied 10-days average air temperature, 10-days average wind speed, 10-days accumulated precipitation and 10-days accumulated sunshine duration prior to the sampling dates.

2.3. Abiotic and phytoplankton data collection

Water depth was measured with a Speedtech SM-5 Depthmate portable sounder (Speedtech Instruments, Great Falls, VA, USA). Water temperature (WT), pH, dissolved oxygen (DO) and electrical conductivity (EC) were measured *in situ* at 0.5 m intervals using a multiparameter water quality analyzer (Hydrolab DS5, Hach company, Loveland, CO, USA). Total carbon (TC) and total organic carbon (TOC) were determined using a Shimadzu TOC-VCPH analyzer (Shimadzu, Japan). Ammonium nitrogen ($\text{NH}_4\text{-N}$), nitrate nitrogen ($\text{NO}_3\text{-N}$), nitrite nitrogen ($\text{NO}_2\text{-N}$) and phosphate phosphorus ($\text{PO}_4\text{-P}$) were analyzed by spectrophotometry. Total nitrogen (TN) and total phosphorus (TP) were measured by spectrophotometry after digestion (Greenberg et al., 1992). Water transparency was measured with a 30 cm diameter Secchi disk. Depth of euphotic zone

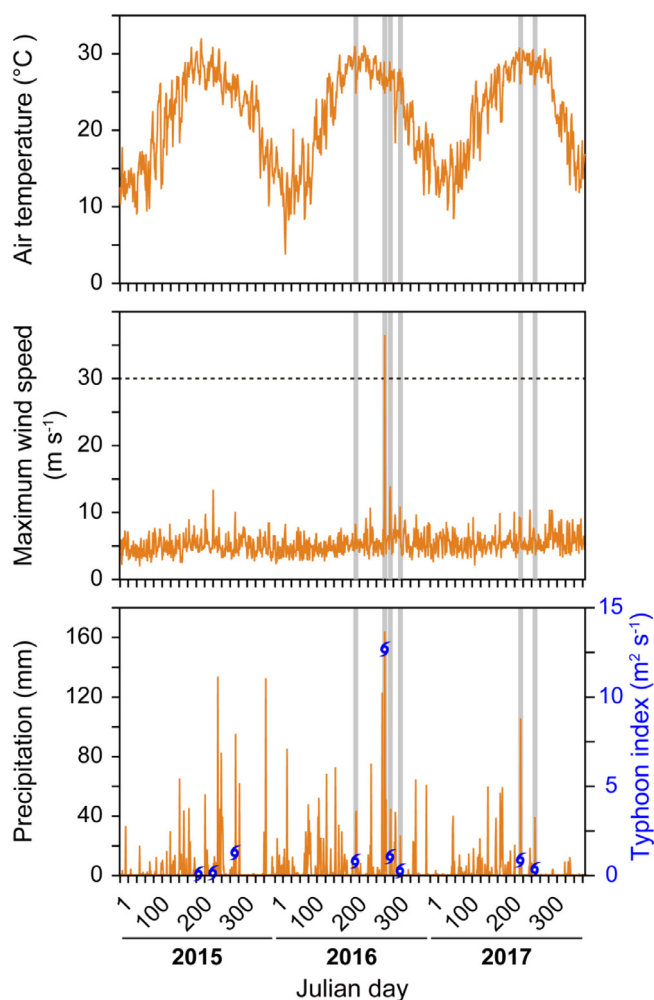


Fig. 1. Air temperature, maximum wind speed, precipitation and typhoon (tropical cyclone) records in Xiamen city, China. Typhoon index is defined as the product of maximal wind speed (m s^{-1}) and past 10 days accumulated precipitation (m) before typhoon events. Typhoon symbols indicate the typhoon index. The shadow areas represent the typhoon events in this study.

(Ze) was estimated as 2.7 times the Secchi depth (Cole, 1994). The masses of the nano- and pico-POM size classes were sampled by sequential filtering of the samples through $20 \mu\text{m}$, $3 \mu\text{m}$ and $0.2 \mu\text{m}$ pore-size polycarbonate filters (47 mm diameter, Millipore, Billerica, MA, USA), respectively. Subsequently, the filters were weighed after drying at 50°C for at least 72 h.

Chlorophyll-*a* and F_v/F_m of blue-green (cyanobacteria), green (chlorophytes) and brown (mostly diatoms and dinoflagellates) algae and the total phytoplankton were measured *ex situ* with a PHYTO-PAM Phytoplankton Analyzer (Heinz Walz GmbH, Effeltrich, Germany). The chlorophyll fluorescence parameter F_v/F_m indicates the maximum quantum efficiency of photosystem II (PSII) photochemistry and can be used as an early disturbance indicator in algae (Dittami et al., 2016). The dominant algal groups were counted using a Flowsight cytometer (Amnis, Merck Millipore, Darmstadt, Germany) equipped with blue-green (488 nm, 60 mV) and side-ward scatter (SSC) (785 nm, 12 mV) solid-state lasers and high image resolution ($20 \times$ magnification). The analyses were performed on Amnis IDEAS software (version 6.2). Red autofluorescence of photosynthetic pigments and SSC were used to distinguish the algae from dead particles. Red and yellow autofluorescences were defined as algal group 1 and group 2, respectively.

2.4. Stable isotopes and stoichiometry of particulate organic matter

Percent carbon, percent nitrogen and $\delta^{13}\text{C}$ and $\delta^{15}\text{N}$ of POM samples were measured using a Thermo Electron Flash EA 2000 elemental analyzer (EA) coupled to a Delta V isotope ratio mass spectrometer (IRMS) (Thermo Fisher Scientific Inc., Waltham, MA, USA). Carbon and nitrogen stable isotope ratios were presented as $\delta^{13}\text{C}$ and $\delta^{15}\text{N}$ relative to Vienna Pee Dee Belemnite carbonate and atmospheric N_2 isotopes, respectively (Fry, 2006). Average analytical errors for $\delta^{13}\text{C}$ and $\delta^{15}\text{N}$ were approximately 0.13‰ and 0.1‰, respectively, in this study. We used the carbon content and C:N ratios to correct the $\delta^{13}\text{C}$ of the net-POM for lipid bias (Syväranta and Rautio, 2010). Other POM size classes typically consisted of algae or bacteria, and the carbon content (C%) of these POM samples was almost less than 40% in our study. Therefore, we did not correct the $\delta^{13}\text{C}$ of the other POM size classes following the method of a previous study (Post et al., 2007). All stoichiometric ratios were calculated using the elemental content of POM.

2.5. Analysis of temporal changes in water parameters

To track the ecological consequences of typhoon events, samples taken within one month before and after typhoon events were selected as pre- and post-typhoon periods, respectively (Table S1). Since the different POM size classes from different water layers were only available from 2016 to 2017, further data analyses were thus performed based on data from the two years. We compared the differences in nutrients between pre- and post-typhoon periods using the nonparametric Mann-Whitney *U* test. The effects of typhoon and water depth on the $\delta^{13}\text{C}$, $\delta^{15}\text{N}$ and stoichiometry of the different POM size classes were evaluated by two-way PERMANOVA analyses in PAST v3.0.

2.6. Multi-nutrient cycling index

The multi-nutrient cycling index was calculated to track the cycling of multiple nutrients. It is analogous to the widely used multi-functionality index for nutrient cycling in terrestrial ecosystems (Maestre et al., 2012; Delgado-Baquerizo et al., 2016; Jiao et al., 2018). We constructed the multi-nutrient cycling index including eight measured nutrient properties: total carbon (TC), total organic carbon (TOC), total nitrogen (TN), ammonium nitrogen ($\text{NH}_4\text{-N}$), nitrate nitrogen ($\text{NO}_3\text{-N}$), nitrite nitrogen ($\text{NO}_2\text{-N}$), total phosphorus (TP) and phosphate phosphorus ($\text{PO}_4\text{-P}$). To quantify the multi-nutrient cycling index for each sample, we first normalized (log-transformed) and then standardized each of the eight nutrient properties using Z-score transformation. The standardized functions were then averaged to obtain the multi-nutrient cycling index.

2.7. Indicators of multi-nutrient cycling

We assessed Spearman's correlation coefficients between stable isotopes and the stoichiometry of different POM size classes and nutrients along the water column. Then, the key predictors for the multi-nutrient cycling index were explored using random forest regression analyses. The analyses were conducted using the *randomForest* package in R environment (R Core Team, 2019). The higher mean square error (MSE) value indicates the variable is more important. We applied the *A3* package to calculate the significance and cross-validated R^2 values with 5000 permutations of the response variables. We simultaneously evaluated the significance of each predictor for the multifunctionality index using the *rfPermute* package.

2.8. Direct and indirect effects of key drivers on multi-nutrient cycling

Finally, we constructed partial least squares path models (PLS-PM) using the *plspm* package to illustrate the direct and indirect effects of the drivers on the multi-nutrient cycling index in the surface, middle and bottom waters, respectively. The drivers were categorized into 7 block variables: meteorological factors (meteo), physicochemical factors (env), algae properties (algae), the mass of POM (Mass), $\delta^{13}\text{C}$, $\delta^{15}\text{N}$ and stoichiometry (stoichio). We did not consider the complex relationships among $\delta^{13}\text{C}$, $\delta^{15}\text{N}$ and stoichiometry. In our initial PLS-PM structure equation, meteorological factors (average 10-days) included precipitation, sunshine, air temperature and wind speed; physicochemical factors included water depth, water level fluctuation, euphotic depth, water temperature, pH, dissolved oxygen and electrical conductivity; algae properties included chlorophyll-*a* and the F_v/F_m of algae groups. We removed the variables with loadings < 0.7 ; goodness of fit index (GoF) and R^2 were used to estimate model performance (Gao et al., 2019). Random forest and PLS-PM analyses were used as complementary approaches to identify the complex relationship between environmental drivers and the multi-nutrient cycling following typhoon events. Random forest analysis does not require the *a priori* hypotheses that are needed in the initial PLS-PM analyses, and it is therefore not limited by previous knowledge. However, PLS-PM can be used to partition the direct and indirect effects of the predictors on the multi-nutrient cycling index.

3. Results

3.1. Meteorological conditions

Most typhoons reach our study site, Tingxi Reservoir, from July to October (Table S1). In this study, four (Nepartak, Meranti, Megi and Haima) and two (Haitang and Mawar) typhoons were observed within a distance of < 300 km from the typhoon center to Tingxi Reservoir in 2016 and 2017, respectively. Of these, Nepartak was the first typhoon with an accumulated 10-days precipitation of 97.3 mm and a maximum wind speed of 7.8 m s^{-1} (Fig. 1). Meranti was the strongest typhoon with a typhoon index $> 12.5 \text{ m}^2 \text{ s}^{-1}$, an accumulated precipitation of 348.3 mm and a maximum wind speed of 36.4 m s^{-1} (Fig. 1; Table S1). These typhoons were typically accompanied by a decrease in air temperature and sunshine hours, and increased local wind speed and precipitation. However, the meteorological conditions recovered rapidly, within one or two days after the typhoon events.

3.2. Variations in nutrients and phytoplankton

The typhoons significantly changed the nutrients in the deep waters (Fig. 2) and deepened the thermocline of the reservoir (Fig. S1c). While the nutrient concentrations were relatively stable in the surface waters, the concentration of nitrate nitrogen ($\text{NO}_3\text{-N}$) was significantly lower after the typhoons in the middle waters (Fig. 2), and the concentration did not reach previous levels until 23 days after the typhoon Haima (Fig. S2; Table S1). The concentration of $\text{NH}_4\text{-N}$, by contrast, was significantly higher in the bottom waters after typhoon events (Fig. 2). The concentrations of TN, $\text{NH}_4\text{-N}$ and total phosphorus (TP) doubled in the bottom waters with a steep increase within the first month after the typhoons Haima and Mawar in 2016 and 2017, respectively (Fig. S2). The pico- and nano-phytoplankton abundances increased sharply in the surface waters of the reservoir after the typhoon Meranti in 2016, while a small increase was recorded after the typhoon Haitang in 2017 (Fig. S3). The responses of algae to typhoons varied

between different algal groups. But for all size classes, algal abundances had recovered in the surface waters within the first month after the typhoons (Fig. S3).

3.3. Stable isotopes and stoichiometry of particulate organic matter

We found that the mass of pico-POM increased significantly in the bottom waters after typhoon events (Fig. 3) and a steep increase occurred following the typhoons Haima and Mawar in 2016 and 2017, respectively (Fig. S4). The $\delta^{13}\text{C}$ values displayed slight decrease in every size class and showed low ability to recover from the typhoons in the surface waters (Fig. 3; Fig. S5), whereas the values were relatively stable and recovered rapidly in the middle and bottom waters after typhoons (Fig. S6). The average $\delta^{13}\text{C}$ of nano-POM displayed a decrease of 3.1‰ in the surface waters (Fig. S5), although the decrease was not significant (Fig. 3). By contrast, the $\delta^{15}\text{N}$ of POM in the surface waters was relatively stable but decreased in the middle and bottom waters after typhoon events (Fig. 3; Fig. S5). Overall, the $\delta^{15}\text{N}$ values of pico-POM were more sensitive to typhoons than other size classes (Table 1). The average $\delta^{15}\text{N}$ value of pico-POM had a decrease of $\sim 2.6\text{‰}$ in both middle and bottom waters after typhoon events (Fig. S6), although the decrease was not significant (Fig. 3). The $\delta^{15}\text{N}$ of pico- and nano-POM in the middle waters tended to recover within 23 days after the typhoon events (Fig. S6). Contrarily, the lowest $\delta^{15}\text{N}$ values of pico- and nano-POM were observed in the bottom waters after the Meranti typhoon, and the values remained extremely low ($\sim 0\text{‰}$) until the following year.

The C:N ratios were relatively stable for every size class in the surface and middle waters, whereas the value increased significantly for pico-POM in the bottom waters after typhoons (Fig. 3). For pico-POM, the highest C:N ratio in the middle waters was observed after the Megi typhoon, followed by a rapid decrease from 11 to 8 after the Haima typhoon (Fig. S7). For pico- and nano-POM in the bottom waters, the C:N ratios displayed a steep increase and did not recover during the first month after the typhoon events, whereas the C:P and N:P ratios remained low after the typhoons Nepartak and Haitang in 2016 and 2017, respectively. For pico- and net-POM, the $\delta^{13}\text{C}$ and C:N ratios were more similar to those of terrestrial sources after typhoon events in the bottom and middle waters, respectively (Fig. S8). The concentrations of particulate organic carbon, nitrogen and phosphorus exhibited a steep increase within the first month after typhoon events (Fig. S7).

3.4. Potential indicators of nutrient cycling

The $\delta^{13}\text{C}$ of all POM size classes exhibited a positive correlation with total carbon (TC) and total organic carbon (TOC) and a negative correlation with total nitrogen (TN) and nitrate nitrogen ($\text{NO}_3\text{-N}$) in the surface waters ($P < 0.05$, Fig. S9). The $\delta^{15}\text{N}$ values of pico-POM demonstrated the strongest positive correlation with TN and $\text{NO}_3\text{-N}$ in the middle waters. In the bottom waters, the $\delta^{15}\text{N}$, C:P and N:P of pico-POM were negatively correlated with $\text{NH}_4\text{-N}$ and TP, but the C:N and the mass of pico-POM showed a positive correlation with $\text{NH}_4\text{-N}$. The large size classes displayed weak correlations with the concentration of nutrients compared with pico-POM in deep waters.

The $\delta^{13}\text{C}$ of nano- and net-POM and C:P of pico-POM were key indicators in the multi-nutrient cycling index for surface waters, while the chlorophyll-*a* of the green algal group was the important indicator for middle waters (Fig. 4). C:N, N:P and the mass of pico-POM were important indicators in the multi-nutrient cycling index for bottom waters despite of the key role played by electrical conductivity (EC) and the F_v/F_m of the brown algal group. Overall, pico-POM was the most important factor for the nutrient cycling

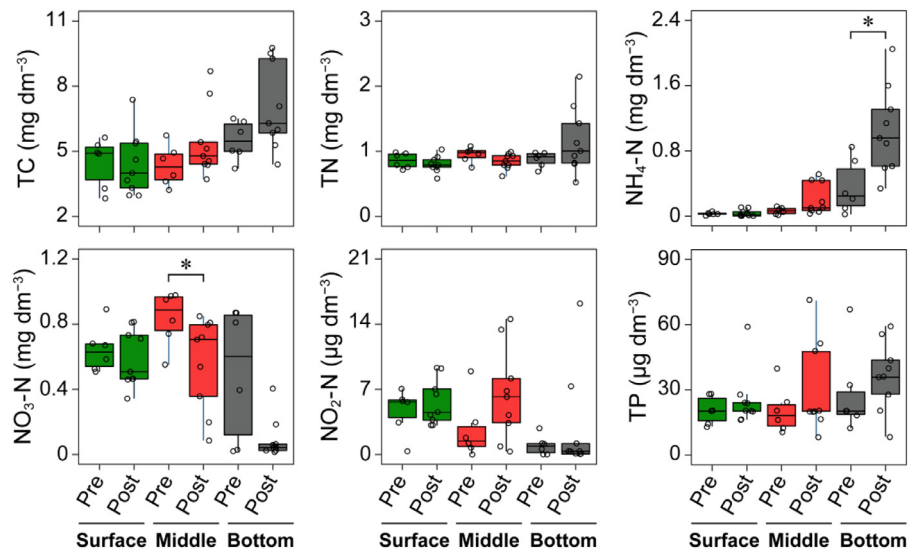


Fig. 2. Comparison of nutrients between the pre- and post-typhoon periods along water column in Tingxi Reservoir. Statistical analysis is nonparametric Mann-Whitney *U* test (**P* < 0.05). Box boundaries indicate the 25th and 75th percentiles; whiskers represent the 10th and 90th percentiles; the inner horizontal lines are the median. TC, total carbon; TN, total nitrogen; TP, total phosphorus.

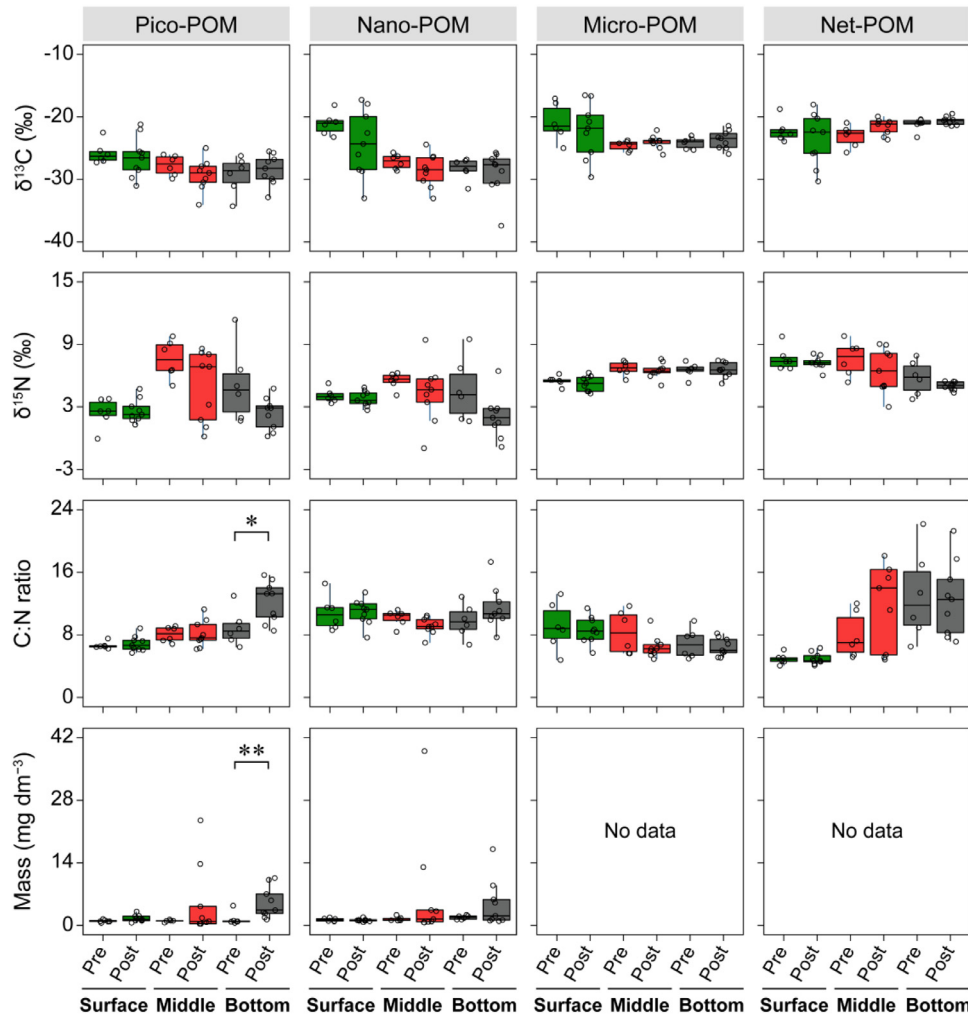


Fig. 3. Comparison of $\delta^{13}\text{C}$, $\delta^{15}\text{N}$, stoichiometry and the mass of particulate organic matter (POM) size classes between the pre- and post-typhoon periods along water column in Tingxi Reservoir. Statistical analysis is nonparametric Mann-Whitney *U* test (**P* < 0.05, ***P* < 0.01). Box boundaries indicate the 25th and 75th percentiles; whiskers represent the 10th and 90th percentiles; the inner horizontal lines are the median. Mass, the mass of POM. Pre, pre-typhoon period; Post, post-typhoon period. Pico-, nano-, micro- and net-POM represent particulate organic matter of the 0.2–3 μm , 3–20 μm , 20–64 μm and 64–200 μm size classes, respectively. All stoichiometric ratios refer to the elemental weight ratios of particulate organic matter.

Table 1

Two-way permutational multivariate analysis of variance (PERMANOVA) showing the effects of typhoon and water depth on $\delta^{13}\text{C}$, $\delta^{15}\text{N}$ and stoichiometry of particulate organic matter.

Grouping by	$\delta^{13}\text{C}$		$\delta^{15}\text{N}$		Stoichiometry	
	F	P	F	P	F	P
Typhoon						
0.2–3 μm	0.284	0.580	5.354	0.017	2.249	0.119
3–20 μm	2.469	0.099	4.360	0.031	0.122	0.727
20–64 μm	0.015	0.901	0.392	0.507	2.540	0.099
64–200 μm	0.081	0.769	3.059	0.075	1.008	0.336
All classes	1.054	0.290	4.440	0.015	1.330	0.226
Depth						
0.2–3 μm	4.095	0.018	8.047	< 0.001	3.245	0.032
3–20 μm	10.751	< 0.001	2.358	0.080	4.334	0.011
20–64 μm	3.812	0.020	12.962	< 0.001	4.827	0.008
64–200 μm	3.075	0.040	8.564	< 0.001	4.633	0.004
All classes	6.487	< 0.001	6.357	< 0.001	3.720	0.005
Typhoon \times Depth						
0.2–3 μm	-2.100	0.764	-0.175	0.168	0.439	0.163
3–20 μm	-3.452	0.996	-1.445	0.546	3.967	0.016
20–64 μm	-2.545	0.860	-2.444	0.916	0.640	0.079
64–200 μm	-1.845	0.645	-1.406	0.523	-2.611	0.569
All classes	-2.683	0.957	-0.905	0.328	1.937	0.028

The boldface indicates the significant difference ($P < 0.05$). All classes include four different sized fractions (0.2–3 μm for pico-POM, 3–20 μm for nano-POM, 20–64 μm for micro-POM, 64–200 μm for net-POM).

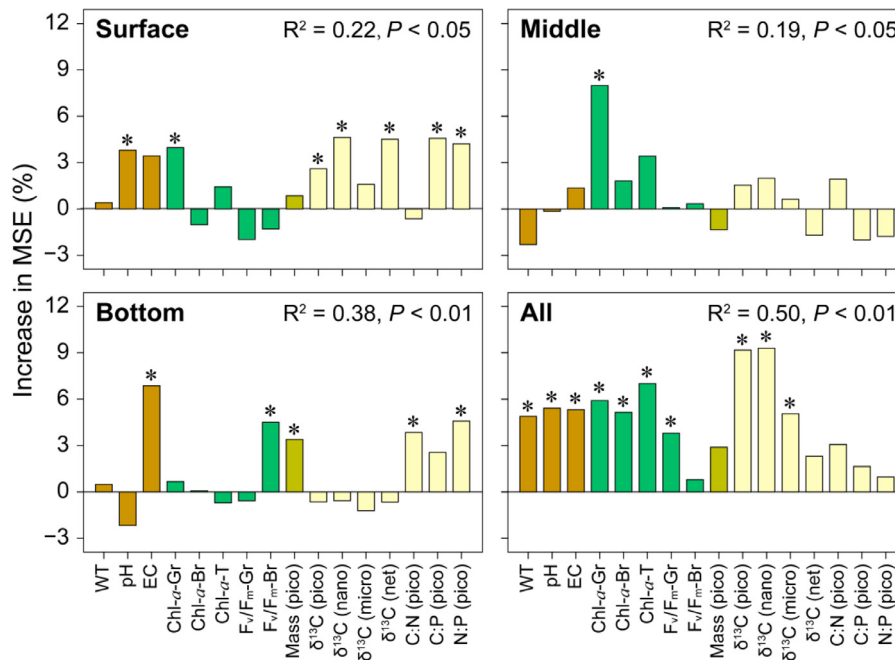


Fig. 4. Main predictors of nutrient cycling variation in different water layers of Tingxi Reservoir. The higher value of mean square error (MSE) indicates greater importance on the multi-nutrient cycling index. The accuracy importance is computed for each tree and averaged over the forest (1000 trees). WT, water temperature; EC, electrical conductivity. Chl-*a*-Gr, Chl-*a*-Br and Chl-*a*-T represent the chlorophyll-*a* of green, brown and all algal groups, respectively. F_v/F_m -Gr and F_v/F_m -Br represent the F_v/F_m of green and brown algal groups. Mass, the mass of particulate organic matter. Pico, nano, micro and net represent particulate organic matter of the 0.2–3 μm , 3–20 μm , 20–64 μm and 64–200 μm size classes, respectively. The drivers are shown in the figures as long as the variables are significant predictors in surface, middle, bottom and all water layers, respectively.

of bottom waters (Fig. 4; Fig. S9). The $\delta^{13}\text{C}$ of pico- and nano-POM were found to be important indicators in the multi-nutrient cycling index, followed by chlorophyll-*a* throughout the water column (Fig. 4).

The multi-nutrient cycling index was well explained by our partial least squares path modeling (PLS-PM) in the surface ($R^2 = 0.41$), middle ($R^2 = 0.79$), bottom ($R^2 = 0.83$) and all water layers ($R^2 = 0.43$) (Fig. S10). For surface waters, the $\delta^{13}\text{C}$ and stoichiometry of POM had a direct but non-significant effect on the multi-nutrient cycling index, while the meteorological factors

exerted a direct effect on the algae and an indirect effect on the multi-nutrient cycling index (Fig. 5). For the middle waters, the $\delta^{13}\text{C}$ and $\delta^{15}\text{N}$ of POM were the most important drivers having a direct and significant effect on the multi-nutrient cycling index. For the bottom waters, the $\delta^{13}\text{C}$, $\delta^{15}\text{N}$, and mass of POM were the main drivers with direct and significant effect on the multi-nutrient cycling index; and algae exerted a strong and indirect effect on the multi-nutrient cycling index through $\delta^{15}\text{N}$ and mass of POM (Fig. 5; Fig. S10). For the whole water column, meteorological factors, physicochemical factors, $\delta^{13}\text{C}$ and the mass of POM had

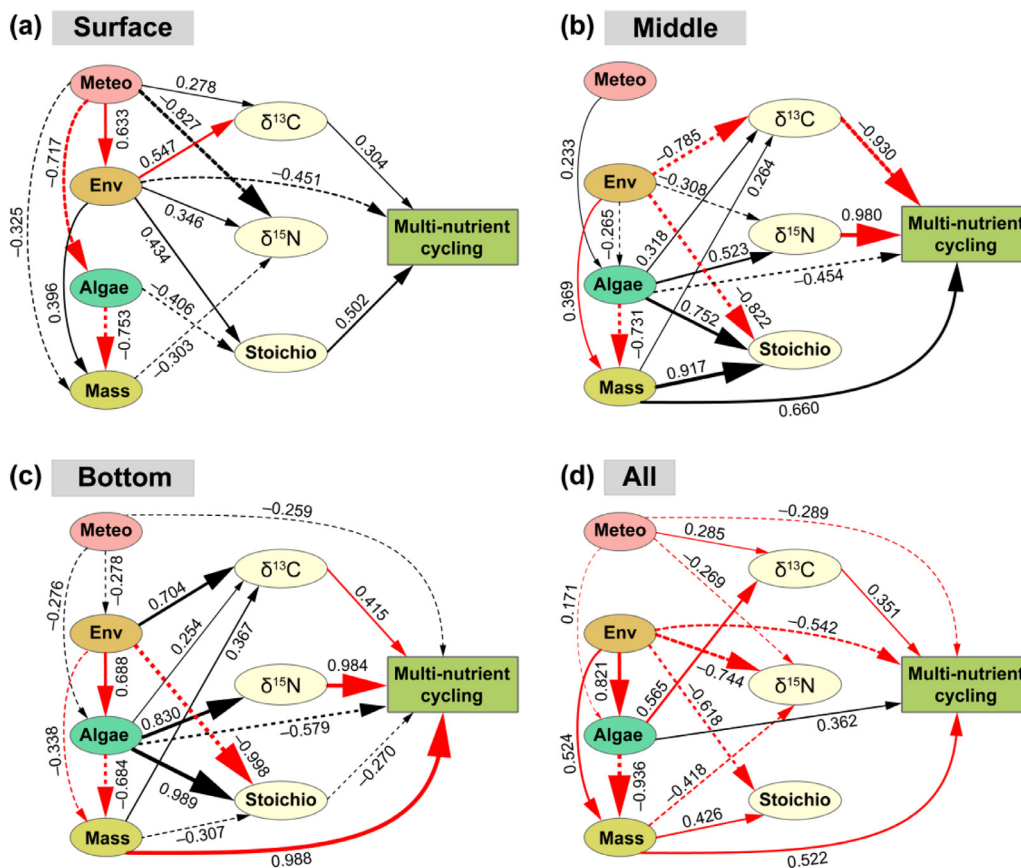


Fig. 5. The final partial least squares path models (PLS-PM) showing relationships between the drivers and the multi-nutrient cycling index in different water layers. Only paths with a coefficient greater than 0.25 are shown with exception of the path from meteorological factors to algae in (b) and (d). Solid and dashed lines represent positive and negative effects, respectively. Red lines represent significant paths ($P < 0.10$). The thickness of the line represents the absolute value of the path coefficients. The goodness-of-fit index for (a)-(d) are 0.649, 0.660, 0.669 and 0.605, respectively. All data are log-transformed except pH and multi-nutrient cycling index. Meteo, meteorological factors; Env, physicochemical factors; Mass, the mass of particulate organic matter; Stoichio, stoichiometry of particulate organic matter.

a direct and significant effect on the multi-nutrient cycling index (Fig. 5).

4. Discussion

4.1. The prolonged response of deep waters to typhoon events

Although previous studies have shown distinct responses of plankton communities and ecosystem metabolism to artificial mixing disturbances between upper and deep waters (Shade et al., 2011, 2012; Giling et al., 2017), the response of these waters to typhoon events is poorly understood, especially for the deep reservoirs (> 30 m). We found that nutrients and POM exhibited a more prolonged response to typhoon events in the bottom than in the surface and middle waters of the reservoir we studied. Furthermore, the events were accompanied by strong mixing disturbance that deepened the thermocline and the hypoxic boundary. The thermocline re-established one day after the typhoons, which was faster than typically found in artificial mixing experiments (Shade et al., 2012; Giling et al., 2017). Unlike the artificial mixing disturbances, typhoons typically bring large amounts of dissolved and particulate nutrients into aquatic ecosystems through runoff (Paerl et al., 2006; Tseng et al., 2010; Johnson et al., 2018). The C:N and $\delta^{13}\text{C}$ values of the pico- and net-POM in the bottom and middle waters, respectively, were similar to those of terrestrial organic matter (TOM) after typhoon events, indicating input and decomposition of TOM in deep waters (Fig. S8). Similarly, we found depleted $\delta^{15}\text{N}$ values of the pico- and nano-POM following typhoon

events, suggesting that ^{15}N -depleted TOM contributed to the nitrogen cycling processes in bottom waters. Further, the significant correlation between $\delta^{15}\text{N}$ and nutrient cycling provided evidence of a distinct nitrogen cycling following typhoon events in deep waters. The decomposition and nitrogen cycling processes are typically controlled by the input of terrestrial organic matter and the microbial communities (Gu, 2009).

Particulate organic matter sinking from the surface to bottom waters is another important contributor to the biogeochemical processes of deep waters (Paerl et al., 2006; Schlesinger and Bernhardt, 2013). Although the algal abundance did not change and remained low in the bottom waters after typhoon events, the concentration and mass of POM (algae and dead organic matter) in the bottom waters increased steeply after the typhoons, most notable in 2016 (Fig. S3; Fig. S4), indicating that most of the algae in the bottom waters were senescent, being undetected in the autofluorescence based chlorophyll-*a* measurement. Further, sediment resuspension might contribute to the increase in POM and thus the nutrient cycling in bottom waters, especially immediately after the strong typhoon. If sediment resuspension was the main contributor to the increase in the POM concentration of bottom waters, the concentration and mass of POM should have been higher in the bottom than in the middle waters. However, we found that the concentration and mass of POM were higher in the middle than bottom waters during the first 10 days after typhoons Meranti and Megi in 2016 (Fig. S3; Fig. S4), indicating that the contribution of sediment resuspension was less than particle sinking already 3 days after the typhoons. This is further supported by the fact that

the concentration and mass of POM increased steeply immediately after the typhoons and then recovered to the pre-disturbance level again within the first month after the typhoons in the middle waters, concurrent with an accumulation and a prolonged increase in chlorophyll-*a* and the mass of POM in the bottom waters (Fig. S2; Fig. S4). Moreover, our random forest regression (Fig. 4) and final partial least squares path models (Fig. 5) indicated the algae (i.e., chlorophyll-*a* and F_v/F_m) played a key role in the particulate organic matter dynamics and nutrient cycling in the middle and bottom waters. Therefore, we assume that typhoon-driven disturbance contributed substantially to the biogeochemical processes of deep waters through increased algae sinking. Overall, the increased organic matter input, algae sinking and subsequent decomposition may explain the steep accumulation of nutrients (e.g., carbon, nitrogen and phosphorus) and prolonged response of the bottom water ecosystem to the typhoon-induced disturbances.

4.2. Small-sized POM is a key nutrient cycling indicator in bottom waters

Our result indicated that small-sized or pico-sized POM (i.e., 0.2–3 μm) was a key indicator of the nutrient cycling in bottom waters. Many studies, mostly focusing on specific taxonomic groups, have shown large variations in plankton communities following typhoons in subtropical lakes and reservoirs (Jones et al., 2008; Tseng et al., 2013; Ko et al., 2017; Stockwell et al., 2020). However, the response of different taxonomic groups to typhoon events can vary with size and chemical composition (e.g., C:N ratio) (Johnson et al., 2018). Here, we assessed the key drivers of nutrient cycling along the water column using different POM size classes covering the entire size spectrum of the taxonomic groups of microbial plankton. We found a steep increase in mass and particulate organic carbon, nitrogen and phosphorus of pico-POM in the bottom waters after the typhoons. This was consistent with the ^{15}N -depleted POM and a steep increase of $\text{NH}_4\text{-N}$ concentrations after typhoons, which may reflect a higher release rate of ^{15}N -depleted $\text{NH}_4\text{-N}$ from the TOM and the uptake by the small-sized POM. Supporting this view, Shade et al. (2012) reported an increasing activity of bacteria in deep waters after an artificial mixing disturbance. Although the community structure can recover after typhoon-induced disturbances (Jones et al., 2008; Ji et al., 2018), the microbially mediated nutrient cycling processes showed a prolonged response to typhoon events in our study reservoir. Furthermore, the bacteria and microalgae have been shown to accumulate polyphosphate by the luxury uptake of phosphorus in waters (Khoshmanesh et al., 2002; Powell et al., 2009). This can explain the accumulation of total phosphorus and the particulate organic phosphorus in pico-POM but not phosphate, especially in deep waters after typhoons. The ecological consequences of typhoon events in deep lakes/reservoirs have been increasingly studied, not least through artificial mixing experiments (Shade et al., 2012; Giling et al., 2017). However, natural typhoon-driven disturbances have more complicated ecological consequences compared with artificial mixing disturbances and particulate organic matter of different sizes should be considered when elucidating the pathways and key drivers of the nutrient cycling in deep waters affecting the ecosystem functioning in a changing environment.

The C:N ratio is a key indicator of the bottom-up energy-matter transfer efficiency (Sardans et al., 2012). However, the increased organic matter input and decomposition promoted by typhoons may cause large variations in elemental concentrations and the C:N ratio of POM in freshwater ecosystems (Paerl et al., 2006; Sterner et al., 2007; Sardans et al., 2012; Johnson et al., 2018). We found a high C:N ratio of pico-POM in the bottom waters after typhoon events. The typhoon-driven increase in the C:N ratio of pico-POM may reduce the energy transfer efficiency across trophic

levels and accelerate the heterotrophic decomposition in deep waters. This may increase the decomposition processes and organic matter mineralization and thus augment $\text{NH}_4\text{-N}$ concentration in deep waters (Schlesinger and Bernhardt, 2013; Chen et al., 2020).

4.3. Implications for water resource management and conservation

Typhoons can facilitate nutrient cycling and accumulation in deep waters, thereby increasing the risk of eutrophication and cyanobacterial dominance of the drinking water reservoir and downstream waters (Stockwell et al., 2020). The steep and prolonged increases of total nitrogen, ammonium nitrogen and total phosphorus in the bottom waters of the deep reservoir after typhoons could increase the risk of the eutrophication development and cyanobacterial dominance when these nutrients eventually reach the surface waters after mixing disturbances. The typhoon-driven higher release rate of $\text{NH}_4\text{-N}$ along with depletion in oxygen due to the mineralization may promote the release of phosphorus by stimulating alkaline phosphatase activity (Ma et al., 2018). We did find an increased algal abundance in surface waters after the typhoons, although there was no significant increase in the chlorophyll-*a* concentration, likely reflecting that algal groups differ in chlorophyll-*a* quantities per cell (Canfield et al., 2019). The cyanobacteria can be fueled by ammonium in the surface water and recovered quickly after typhoon (Chen et al., 2018), and the algae sinking, in turn, acts as important source for nutrient accumulation in the deep waters. Thus, the increased typhoon-driven organic matter input and nutrient cycling in the bottom waters potentially drive harmful algal blooms in deep reservoirs (Maavara et al., 2020), and increase export of the bioavailable nutrients to downstream waters (Chen et al., 2020) and cause serious water quality problems. In this study, we focus on the short-term effect of typhoon, but longer-term high-resolution sampling is needed to gain a better understanding of the differential effect of different typhoons and potential carry-over effect from one typhoon to the next.

5. Conclusions

This study evaluated the ecological consequences of typhoon events by combining stable isotope and stoichiometry analyses with a multi-nutrient cycling index in a subtropical deep reservoir. We found a more prolonged response of nutrients and POM in the bottom than in the surface and middle waters following typhoon events. The connectivity between surface and deep waters through sinking algae could partially explain the prolonged responses of POM and nutrients in the bottom waters. The increased C:N ratio of small-sized or pico-sized POM (i.e., 0.2–3 μm) driven by typhoons may have inhibited the bottom-up energy-matter transfer efficiency and accelerated the heterotrophic decomposition in deep waters. The pico-POM was a key contributor to the enhanced nutrient cycling in deep waters. The organic matter input, algae sinking and heterotrophic bacteria interacted with each other to cause the steep and prolonged increases of total nitrogen, ammonium nitrogen and total phosphorus in the bottom waters of the reservoir. The increasing intensity of typhoons might increase the risk of eutrophication and cyanobacterial blooms in a future warmer climate.

Declaration of Competing Interest

The authors declare that they have no known competing financial interests or personal relationships that could have appeared to influence the work reported in this paper.

Acknowledgements

We thank Jean Claude Ndayishimiye and Anne Mette Poulsens for comments on an earlier version of this paper. The work was funded by the [National Natural Science Foundation of China](#) (91851104, 31672312 and 41703074) and the Natural Science Foundation of Fujian Province of China (2019J02016).

Supplementary materials

Supplementary material associated with this article can be found, in the online version, at [doi:10.1016/j.watres.2020.116470](https://doi.org/10.1016/j.watres.2020.116470).

References

- Boehrer, B., Schultze, M., 2008. Stratification of lakes. *Rev. Geophys.* 46, RG2005. doi:[10.1029/2006RG000210](https://doi.org/10.1029/2006RG000210).
- Canfield Jr, D.E., Bachmann, R.W., Hoyer, M.V., Johansson, L.S., Søndergaard, M., Jeppesen, E., 2019. To measure chlorophyll or phytoplankton biovolume: an aquatic conundrum with implications for the management of lakes. *Lake Reserv. Manage.* 35, 181–192. doi:[10.1080/10402381.2019.1607958](https://doi.org/10.1080/10402381.2019.1607958).
- Chen, N.W., Mo, Q.L., Kuo, Y.M., Su, Y.P., Zhong, Y.P., 2018. Hydrochemical controls on reservoir nutrient and phytoplankton dynamics under storms. *Sci. Total Environ.* 619–620, 301–310. doi:[10.1016/j.scitotenv.2017.09.216](https://doi.org/10.1016/j.scitotenv.2017.09.216).
- Chen, Q.W., Shi, W.Q., Huisman, J., Maberly, S.C., Zhang, J.Y., Yu, J.H., Chen, Y.C., Tonina, D., Yi, Q.C., 2020. Hypolimnetic reservoirs on the upper Mekong River modify nutrient bioavailability downstream. *Natl. Sci. Rev.* 7, 1449–1457. doi:[10.1093/nsr/nwaa026](https://doi.org/10.1093/nsr/nwaa026).
- Chételat, J., Pick, F.R., Hamilton, P.B., 2006. Potamoplankton size structure and taxonomic composition: influence of river size and nutrient concentrations. *Limnol. Oceanogr.* 51, 681–689. doi:[10.4319/lo.2006.51.1.part_2.0681](https://doi.org/10.4319/lo.2006.51.1.part_2.0681).
- Cole, G.A., 1994. *Textbook of Limnology: Prospect Heights*. Waveland Press, Illinois, USA.
- Coumou, D., Rahmstorf, S., 2012. A decade of weather extremes. *Nat. Clim. Change* 2, 491–496. doi:[10.1038/nclimate1452](https://doi.org/10.1038/nclimate1452).
- Delgado-Baquerizo, M., Maestre, F.T., Reich, P.B., Jeffries, T.C., Gaitan, J.J., Encinar, D., Berdugo, M., Campbell, C.D., Singh, B.K., 2016. Microbial diversity drives multifunctionality in terrestrial ecosystems. *Nat. Commun.* 7, 10541. doi:[10.1038/ncomms10541](https://doi.org/10.1038/ncomms10541).
- Dittami, S.M., Duboscq-Bidot, L., Perennou, M., Gobet, A., Corre, E., Boyen, C., Tonon, T., 2016. Host-microbe interactions as a driver of acclimation to salinity gradients in brown algal cultures. *ISME J.* 10, 51–63. doi:[10.1038/ismej.2015.104](https://doi.org/10.1038/ismej.2015.104).
- Elsler, J.J., Urabe, J., 1999. The stoichiometry of consumer-driven nutrient recycling: theory, observations, and consequences. *Ecology* 80, 735–751. doi:[10.1890/0012-9658\(1999\)080\[0735:TSCODN\]2.0.CO;2](https://doi.org/10.1890/0012-9658(1999)080[0735:TSCODN]2.0.CO;2).
- Emanuel, K., 2020. Evidence that hurricanes are getting stronger. *Proc. Natl Acad. Sci. USA* 117, 13194–13195. doi:[10.1073/pnas.2007742117](https://doi.org/10.1073/pnas.2007742117).
- Fang, Q.H., 2016. Adapting Chinese cities to climate change. *Science* 354, 425–426. doi:[10.1126/science.aak9826](https://doi.org/10.1126/science.aak9826).
- Fry, B., 2006. *Stable Isotope Ecology*. Springer, New York, USA.
- Gao, X.F., Chen, H.H., Govaert, L., Wang, W.P., Yang, J., 2019. Responses of zooplankton body size and community trophic structure to temperature change in a subtropical reservoir. *Ecol. Evol.* 9, 12544–12555. doi:[10.1002/ece3.5718](https://doi.org/10.1002/ece3.5718).
- Giling, D.P., Nejtgaard, J.C., Berger, S.A., Grossart, H.P., Kirillin, G., Penske, A., Lentz, M., Casper, P., Sareyka, J., Gessner, M.O., 2017. Thermocline deepening boosts ecosystem metabolism: evidence from a large-scale lake enclosure experiment simulating a summer storm. *Global Change Biol.* 23, 1448–1462. doi:[10.1111/gcb.13512](https://doi.org/10.1111/gcb.13512).
- Glibert, P.M., Middelburg, J.J., McClelland, J.W., Zanden, M.J.V., 2019. Stable isotope tracers: enriching our perspectives and questions on sources, fates, rates, and pathways of major elements in aquatic systems. *Limnol. Oceanogr.* 64, 950–981. doi:[10.1002/lno.11087](https://doi.org/10.1002/lno.11087).
- Greenberg, A.E., Clesceri, L.S., Eaton, A.D., 1992. *Standard Methods for the Examination of Water and Wastewater*. American Public Health Association, Washington, USA.
- Gu, B.H., 2009. Variations and controls of nitrogen stable isotopes in particulate organic matter of lakes. *Oecologia* 160, 421–431. doi:[10.1007/s00442-009-1323-z](https://doi.org/10.1007/s00442-009-1323-z).
- Gu, B.H., Chapman, A.D., Schelske, C.L., 2006. Factors controlling seasonal variations in stable isotope composition of particulate organic matter in a softwater eutrophic lake. *Limnol. Oceanogr.* 51, 2837–2848. doi:[10.4319/lo.2006.51.6.2837](https://doi.org/10.4319/lo.2006.51.6.2837).
- Gu, B.H., Schelske, C.L., Waters, M.N., 2011. Patterns and controls of seasonal variability of carbon stable isotopes of particulate organic matter in lakes. *Oecologia* 165, 1083–1094. doi:[10.1007/s00442-010-1888-6](https://doi.org/10.1007/s00442-010-1888-6).
- Ji, G., Havens, K.E., Beaver, J.R., East, T.L., 2018. Recovery of plankton from hurricane impacts in a large shallow lake. *Freshw. Biol.* 63, 366–379. doi:[10.1111/fwb.13075](https://doi.org/10.1111/fwb.13075).
- Jiao, S., Chen, W.M., Wang, J.L., Du, N.N., Li, Q.P., Wei, G.H., 2018. Soil microbiomes with distinct assemblies through vertical soil profiles drive the cycling of multiple nutrients in reforested ecosystems. *Microbiome* 6, 146. doi:[10.1186/s40168-018-0526-0](https://doi.org/10.1186/s40168-018-0526-0).
- Johnson, E.R., Inamdar, S., Kan, J., Vargas, R., 2018. Particulate organic matter composition in stream runoff following large storms: role of POM sources, particle size, and event characteristics. *J. Geophys. Res. Biogeosci.* 123, 660–675. doi:[10.1002/2017JG004249](https://doi.org/10.1002/2017JG004249).
- Jones, S.E., Chiu, C., Kratz, T.K., Wu, J.T., Shade, A., McMahon, K.D., 2008. Typhoons initiate predictable change in aquatic bacterial communities. *Limnol. Oceanogr.* 53, 1319–1326. doi:[10.4319/lo.2008.53.4.1319](https://doi.org/10.4319/lo.2008.53.4.1319).
- Khoshmanesh, A., Hart, B.T., Duncan, A., Beckett, R., 2002. Luxury uptake of phosphorus by sediment bacteria. *Water Res.* 36, 774–778. doi:[10.1016/S0043-1354\(01\)00272-X](https://doi.org/10.1016/S0043-1354(01)00272-X).
- Ko, C.Y., Lai, C.C., Hsu, H.H., Shiah, F.K., 2017. Decadal phytoplankton dynamics in response to episodic climatic disturbances in a subtropical deep freshwater ecosystem. *Water Res.* 109, 102–113. doi:[10.1016/j.watres.2016.11.006](https://doi.org/10.1016/j.watres.2016.11.006).
- Leal, M.C., Seehausen, O., Matthews, B., 2017. The ecology and evolution of stoichiometric phenotypes. *Trends Ecol. Evol.* 32, 108–117. doi:[10.1016/j.tree.2016.11.006](https://doi.org/10.1016/j.tree.2016.11.006).
- Liu, L.M., Chen, H.H., Liu, M., Yang, J.R., Xiao, P., Wilkinson, D.M., Yang, J., 2019. Response of the eukaryotic plankton community to the cyanobacterial biomass cycle over 6 years in two subtropical reservoirs. *ISME J.* 13, 2196–2208. doi:[10.1038/s41396-019-0417-9](https://doi.org/10.1038/s41396-019-0417-9).
- Ma, S.N., Wang, H.J., Wang, H.Z., Li, Y., Liu, M., Liang, X.M., Jeppesen, E., Søndergaard, M., 2018. High ammonium loading can increase alkaline phosphatase activity and promote sediment phosphorus release: a two-month mesocosm experiment. *Water Res.* 145, 388–397. doi:[10.1016/j.watres.2018.08.043](https://doi.org/10.1016/j.watres.2018.08.043).
- Maavara, T., Chen, Q.W., Van Meter, K., Brown, L.E., Zhang, J.Y., Ni, J.R., Zarfl, C., 2020. River dam impacts on biogeochemical cycling. *Nat. Rev. Earth Environ.* 1, 103–116. doi:[10.1038/s43017-019-0019-0](https://doi.org/10.1038/s43017-019-0019-0).
- Maestre, F.T., Quero, J.L., Gotelli, N.J., Escudero, A., Ochoa, V., Delgado-Baquerizo, M., García-Gómez, M., Bowker, M.A., Soliveres, S., Escolar, C., García-Palacios, P., Berdugo, M., Valencia, E., Gzalo, B., Gallardo, A., Aguilera, L., Arredondo, T., Blones, J., Boeken, B., Bran, D., Conceição, A.A., Cabrera, O., Chaieb, M., Derak, M., Eldridge, D.J., Espinosa, C.I., Florentino, A., Gaitán, M., J., Gatica, G., Ghiloufi, W., Gómez-González, S., Gutiérrez, J.R., Hernández, R.M., Huang, X.W., Huber-Sannwald, E., Jankju, M., Miriti, M., Monerri, J., Mau, R.L., Morici, E., Naseri, K., Ospina, A., Polo, V., Prina, A., Pucheta, E., Ramirez-Collantes, D.A., Romão, R., Tighe, M., Torres-Díaz, C., James, Val, Veiga, J.P., Wang, D.L., Zaady, E., 2012. Plant species richness and ecosystem multifunctionality in global drylands. *Science* 335, 214–218. doi:[10.1126/science.1215442](https://doi.org/10.1126/science.1215442).
- Moore, J.C., Berlow, E.L., Coleman, D.C., de Ruiter, P.C., Dong, Q., Hastings, A., Johnson, N.C., McCann, K.S., Melville, K., Morin, P.J., Nadelhoffer, K., Rosemond, A.D., Post, D.M., Sabo, J.L., Scow, K.M., Vanni, M.J., Diana, H., Wall, D.H., 2004. Detritus, trophic dynamics and biodiversity. *Ecol. Lett.* 7, 584–600. doi:[10.1111/j.1461-0248.2004.00606.x](https://doi.org/10.1111/j.1461-0248.2004.00606.x).
- Mumby, P.J., Vitolo, R., Stephenson, D.B., 2011. Temporal clustering of tropical cyclones and its ecosystem impacts. *Proc. Natl Acad. Sci. USA* 108, 17626–17630. doi:[10.1073/pnas.1100436108](https://doi.org/10.1073/pnas.1100436108).
- Paerl, H.W., Valdes, L.M., Peierls, B.L., Adolf, J.E., Harding, L.J.W., 2006. Anthropogenic and climatic influences on the eutrophication of large estuarine ecosystems. *Limnol. Oceanogr.* 51, 448–462. doi:[10.4319/lo.2006.51.1_part_2.0448](https://doi.org/10.4319/lo.2006.51.1_part_2.0448).
- Post, D.M., Layman, C.A., Arrington, D.A., Takimoto, G., Quattrochi, J., Montana, C.G., 2007. Getting to the fat of the matter: models, methods and assumptions for dealing with lipids in stable isotope analyses. *Oecologia* 152, 179–189. doi:[10.1007/s00442-006-0630-x](https://doi.org/10.1007/s00442-006-0630-x).
- Powell, N., Shilton, A., Chisti, Y., Pratt, S., 2009. Towards a luxury uptake process via microalgae—defining the polyphosphate dynamics. *Water Res.* 43, 4207–4213. doi:[10.1016/j.watres.2009.06.011](https://doi.org/10.1016/j.watres.2009.06.011).
- R Core Team, 2019. R: A Language and Environment for Statistical Computing. R Foundation for Statistical Computing, Vienna, Austria <https://www.r-project.org>.
- Sajjad, M., Li, Y., Li, Y., Chan, J.C.L., Khalid, S., 2019. Integrating typhoon destructive potential and social-ecological systems toward resilient coastal communities. *Earth's Future* 7, 805–818. doi:[10.1029/2019EF001226](https://doi.org/10.1029/2019EF001226).
- Sardans, J., Rivas-Ubach, A., Penuelas, J., 2012. The elemental stoichiometry of aquatic and terrestrial ecosystems and its relationships with organismic lifestyle and ecosystem structure and function: a review and perspectives. *Biogeochemistry* 111, 1–39. doi:[10.1007/s10533-011-9640-9](https://doi.org/10.1007/s10533-011-9640-9).
- Schlesinger, W.H., Bernhardt, E.S., 2013. *Biogeochemistry: An Analysis of Global Change*. Academic Press, New York, USA.
- Shade, A., Read, J.S., Youngblut, N.D., Fierer, N., Knight, R., Kratz, T.K., Lottig, N.R., Roden, E.E., Stanley, E.H., Stombaugh, J., Whitaker, R.J., Wu, C.H., McMahon, K.D., 2012. Lake microbial communities are resilient after a whole-ecosystem disturbance. *ISME J.* 6, 2153–2167. doi:[10.1038/ismej.2012.56](https://doi.org/10.1038/ismej.2012.56).
- Shade, A., Read, J.S., Welkie, D.G., Kratz, T.K., Wu, C.H., McMahon, K.D., 2011. Resistance, resilience and recovery: aquatic bacterial dynamics after water column disturbance. *Environ. Microbiol.* 13, 2752–2767. doi:[10.1111/j.1462-2920.2011.02546.x](https://doi.org/10.1111/j.1462-2920.2011.02546.x).
- Sinha, E., Michalak, A.M., Balaji, V., 2017. Eutrophication will increase during the 21st century as a result of precipitation changes. *Science* 357, 405–408. doi:[10.1126/science.aan2409](https://doi.org/10.1126/science.aan2409).
- Sterner, R.W., Anagnostou, E., Brovold, S., Bullerjahn, G.S., Finlay, J.C., Kumar, S., McKay, R.M.L., Sherrell, R.M., 2007. Increasing stoichiometric imbalance in North America's largest lake: nitrification in Lake Superior. *Geophys. Res. Lett.* 34, L10406. doi:[10.1029/2006GL028861](https://doi.org/10.1029/2006GL028861).
- Stockwell, J.D., Doubek, J.P., Adrian, R., Anneville, O., Carey, C.C., Carvalho, L., De Senerpont Domis, L.N., Dur, G., Frassl, M.A., Grossart, H., Ibelings, B.W., Lajeunesse, M.J., Lewandowska, A.M., Llamas, M.E., Matsuzaki, S.S., Nodine, E.R., Nöges, P., Patil, V.P., Pomati, F., Rinke, K., Rudstam, L.G., Rusak, J.A., Salmasso, N., Seltmann, C.T., Straile, D., Thackeray, S.J., Thiery, W., Urrutia-Cordero, P., Veal, N.P., Verburg, P., Woolway, R.I., Zohary, T., Andersen, M.R., Bhattacharya, R., Hejzlar, J., Janatian, N., Kpodonu, A.T.N.K., Williamson, T.J., Wilson, H.L., 2020.

- Storm impacts on phytoplankton community dynamics in lakes. *Global Change Biol.* 26, 2756–2784. doi:[10.1111/gcb.15033](https://doi.org/10.1111/gcb.15033).
- Syväranta, J., Rautio, M., 2010. Zooplankton, lipids and stable isotopes: importance of seasonal, latitudinal, and taxonomic differences. *Can. J. Fish. Aquat. Sci.* 67, 1721–1729. doi:[10.1139/F10-091](https://doi.org/10.1139/F10-091).
- Trochine, C., Guerrieri, M., Liborius, L., Willems, P., Lauridsen, T.L., Søndergaard, M., Jeppesen, E., 2017. Factors controlling the stable isotope composition and C:N ratio of seston and periphyton in shallow lake mesocosms with contrasting nutrient loadings and temperatures. *Freshw. Biol.* 62, 1596–1613. doi:[10.1111/fwb.12971](https://doi.org/10.1111/fwb.12971).
- Tseng, C.H., Chiang, P.W., Shiah, F.K., Chen, Y.L., Liou, J.R., Hsu, T.C., Maheswararajah, S., Saeed, I., Halgamuge, S., Tang, S.L., 2013. Microbial and viral metagenomes of a subtropical freshwater reservoir subject to climatic disturbances. *ISME J.* 7, 2374–2386. doi:[10.1038/ismej.2013.118](https://doi.org/10.1038/ismej.2013.118).
- Tseng, Y.F., Hsu, T.C., Chen, Y.L., Kao, S.J., Wu, J.T., Lu, J.C., Lai, C.C., Kuo, H.Y., Lin, C.S., Yamamoto, Y., Xiao, T., Shiah, F.K., 2010. Typhoon effects on DOC dynamics in a phosphate-limited reservoir. *Aquat. Microb. Ecol.* 60, 247–260. doi:[10.3354/ame01423](https://doi.org/10.3354/ame01423).
- Wang, W.L., Moore, J.K., Martiny, A.C., Primeau, F.W., 2019. Convergent estimates of marine nitrogen fixation. *Nature* 566, 205–211. doi:[10.1038/s41586-019-0911-2](https://doi.org/10.1038/s41586-019-0911-2).
- Woodward, G., Ebenman, B., Emmerson, M., Montoya, J.M., Olesen, J.M., Valido, A., Warren, P.H., 2005. Body size in ecological networks. *Trends Ecol. Evol.* 20, 402–409. doi:[10.1016/j.tree.2005.04.005](https://doi.org/10.1016/j.tree.2005.04.005).
- Yang, J., Lv, H., Yang, J., Liu, L.M., Yu, X.Q., Chen, H.H., 2016. Decline in water level boosts cyanobacteria dominance in subtropical reservoirs. *Sci. Total Environ.* 557/558, 445–452. doi:[10.1016/j.scitotenv.2016.03.094](https://doi.org/10.1016/j.scitotenv.2016.03.094).
- Yang, J., Yu, X.Q., Liu, L.M., Zhang, W.J., Guo, P.Y., 2012. Algae community and trophic state of subtropical reservoirs in southeast Fujian, China. *Environ. Sci. Pollut. Res.* 19, 1432–1442. doi:[10.1007/s11356-011-0683-1](https://doi.org/10.1007/s11356-011-0683-1).
- Yu, Z., Yang, J., Amalfitano, S., Yu, X.Q., Liu, L.M., 2014. Effects of water stratification and mixing on microbial community structure in a subtropical deep reservoir. *Sci. Rep.* 4, 5821. doi:[10.1038/srep05821](https://doi.org/10.1038/srep05821).